

RESEARCH ARTICLE

[View Article Online](#)
[View Journal](#) | [View Issue](#)

 Cite this: *Inorg. Chem. Front.*, 2023, **10**, 5602

The transformation of a zero-dimensional cluster into a one-dimensional chain structure achieving a dramatically enhanced birefringence in tin(II)-based oxalates†

 Liying Ren,^a Linhong Cheng,^a Xiaoyan Zhou,^a Jinxuan Ren,^a Liling Cao,^{id} *^a
 Ling Huang,^{id} ^a Xuehua Dong,^a Yuqiao Zhou,^{id} ^b Daojiang Gao^a and
 Guohong Zou^{id} *^b

Developing new birefringent materials with large optical anisotropy is extremely urgent due to the fantastic progress of laser science and technology. Here, two tin(II)-based oxalates, $K_2Sn(C_2O_4)_2 \cdot H_2O$ and $K_2Sn_2(C_2O_4)_2F_2 \cdot H_2O$, were successfully synthesized by simultaneously introducing π -conjugated $[C_2O_4]^{2-}$ groups and distorted Sn^{2+} -polyhedra with stereochemically active lone pairs. The use of F^- regulates the arrangement of birefringence-active groups, resulting in the transformation of zero-dimensional (0D) $K_2Sn(C_2O_4)_2 \cdot H_2O$ into 1D $K_2Sn_2(C_2O_4)_2F_2 \cdot H_2O$, which successfully enhances birefringence from 0.103@546 nm to 0.301@546 nm. Meaningfully, detailed structural and property analysis demonstrates that the ideal spatial arrangement of all the birefringence-active functional modules can induce strong optical anisotropy, providing an idea for designing birefringent materials with excellent properties.

 Received 29th June 2023,
 Accepted 18th August 2023

DOI: 10.1039/d3qi01213a

rsc.li/frontiers-inorganic

Introduction

Birefringent crystals, an important component of optoelectronic devices, exhibit strong light modulation ability.^{1,2} In particular, crystals with large birefringence play an extremely critical role in both military and civilian applications, such as medical diagnosis, fiber-optic communications, flat panel displays, polarimetry, *etc.*^{3,4} In the past decades, many birefringent crystals, including natural (*e.g.*, quartz crystal, mica, calcite and so on) and artificial (*e.g.*, α -BaB₂O₄ (α -BBO),⁵ MgF₂,⁶ YVO₄⁷ and so on) birefringent crystals, have been discovered and synthesized. Among these some have already gained commercial interest, but their inherent defects, such as unavoidable impurities of natural crystals and low transmittance in the UV region for YVO₄⁷ and CaCO₃,⁸ prevent their application in more advanced miniature optical devices for future markets. Therefore, the pressing need for new optical crystals

with excellent performance, a large birefringence, stable physicochemical properties and easy growth characteristics is driving research efforts.

The birefringence of crystals essentially arises from the anisotropic response of the electron distribution to the applied electric field, and the following groups have been confirmed to enhance the birefringence of compounds due to their strong anisotropic response: (1) π -conjugated planar units, such as H_xBO_3 ($x = 0-3$), H_xCO_3 ($x = 0-2$), $H_xB_3O_6$ ($x = 0-3$), $H_xC_3N_3O_3$ ($x = 0-3$), and $H_xC_3O_4$ ($x = 0-4$).⁹⁻¹⁷ Wang's group reported that $Rb_3Na(H_2C_3N_3O_3)_4 \cdot 3H_2O$ ¹⁸ crystals exhibit a large birefringence of 0.368@1064 nm, which essentially derives from delocalized conjugated orbitals on the planar $(H_2C_3N_3O_3)^-$. (2) Distorted tetrahedral moieties, such as fluorooxoborates $[BO_xF_{4-x}]^{(x+1)-}$ and fluorophosphates PO_3F , which have produced BaB₈O₁₂F₂ (0.116@1064 nm)¹⁹ and $(N_2H_6)[HPO_3F]_2$ (0.077@1064 nm)²⁰ with enhanced birefringence. (3) Jahn-Teller cations include the specifically octahedrally coordinated d^0 transition metals (TMs: Mo⁶⁺, W⁶⁺, V⁵⁺, and Nb⁵⁺) and cations with stereochemically active lone pairs (SCALP, I⁵⁺, Te⁴⁺, Se⁴⁺, and Sn²⁺) such as d^0 transition metal cations Nb⁵⁺ in K₃Nb₃Ge₂O₁₃ (0.196@546 nm)²¹ and (*R*)- and (*S*)-[C₈H₁₀NO₃]₂[NbOF₅] (0.19–0.199@589.3 nm),²² Ti⁴⁺ in BaTi(BO₃)₂ (0.169@546 nm),²³ stereochemically active lone pair (SCALP) cations Sn²⁺ in Sn₂PO₄Br (0.336@546 nm),²⁴ Sb³⁺ in K₂SbP₂O₇F (0.157@546 nm),²⁵ and SbB₃O₆ (0.290@546 nm),²⁶ I⁵⁺ in LiGaF₂(IO₃)₂ (0.206@532 nm).²⁷ The current strategy

^aCollege of Chemistry and Materials Science, Sichuan Normal University, Chengdu 610066, P. R. China. E-mail: llcao21@163.com

^bCollege of Chemistry, Sichuan University, Chengdu 610065, P. R. China. E-mail: zough@scu.edu.cn

 †Electronic supplementary information (ESI) available: Additional crystallographic data, XRD patterns, IR spectra, TGA, the residue of TGA and UV-vis-NIR diffuse reflectance spectra of $K_2Sn(C_2O_4)_2 \cdot H_2O$ and $K_2Sn_2(C_2O_4)_2F_2 \cdot H_2O$. CCDC 2267040 for $K_2Sn(C_2O_4)_2 \cdot H_2O$ and 2267041 for $K_2Sn_2(C_2O_4)_2F_2 \cdot H_2O$. For ESI and crystallographic data in CIF or other electronic format see DOI: <https://doi.org/10.1039/d3qi01213a>

focuses on the simultaneous introduction of multiple birefringence-active functional modules (FMs) mentioned above into one structure to construct optical materials with large birefringence. Noteworthy, the large birefringence is determined not only by the screening of FMs, but also their spatial arrangement. In 2018, Jayakanth Ravichandran *et al.* found that the quasi-one-dimensional (quasi-1D) structural configuration in BaTiS₃ could increase the polarizability anisotropy and favorably bring large birefringence up to 0.76 in the mid- to long-wave infrared region.²⁸ Beyond that, the structural advantages of the 1D configuration are also reflected in Na₂BP₂ (0.68@2000 nm)²⁹ and [C(NH₂)₃]Sb(C₂O₄)F₂·H₂O (0.323@546 nm).³⁰ Hence, selecting suitable FMs to construct 1D structures is a promising strategy to gain crystals with large birefringence.

Obviously, a 1D configuration is an ideal structural framework for obtaining large birefringence as described above. Nevertheless, not all birefringence-active FMs can be constructed into chains, since the formation of chains has an indispensable condition, *i.e.*, FMs with a unique coordination environment can prevent chain-to-chain connection and extension. So how do we effectively screen out the appropriate birefringence-active FMs? In molecular engineering, chemical scissors have been proved to be reliable structure-directing agents in the controlled design of crystal microstructures. To our knowledge, lone pair electrons act as chemical scissors to architecturally shape the target structure in many classical compounds of Pb₂BO₃Cl,³¹ Cs₂Pb(NO₃)₂Br,³² and KSb₂C₂O₄F₅,³³ because cations occupied by lone pair electrons on one side can form highly distorted polyhedra that not only exhibit large anisotropic polarizabilities, but also prevent connection with other structure modules on the same side. The Sn²⁺ cation is a highly promising candidate that, in addition to possessing SCALP, has rich coordination modes (terdentate, quadridentate, quinquidentate, and sexadentate),^{34–36} allowing for increased structural diversity, *e.g.*, Sn₂B₅O₉Cl,³⁷ α-SnF₂,³⁸ K₃Sn₂(SO₄)₃Cl,³⁴ and Sn₂[B₇O₁₂]F.³⁹ In addition, the presence of planar anionic groups is essential for the development of low-dimensional structures because of their unique structural malleability. In recent years, experimental and theoretical evidence from Pan's and Zou's groups has demonstrated that planar C₂O₄²⁻ groups are promising birefringence-active FMs, as exemplified by (NH₄)₂C₂O₄·H₂O,⁴⁰ Na₂Sb₂(C₂O₄)F₆,⁴¹ Cs₂Sb₂(C₂O₄)₂F₄·H₂O⁴¹ and so on. The four O atoms of the C₂O₄²⁻ groups all lie in the same plane, resulting in adjacent groups extending along the plane by sharing O atoms and ultimately forming a low-dimensional structure. In terms of properties, the C₂O₄²⁻ groups exhibit strong π-conjugated interactions due to shorter bond lengths, strong P_π-P_π interactions and additional electron-populated p orbitals provided by C and O atoms, resulting in the production of large anisotropic polarizability and even large birefringence.

Based on the above ideas, the Sn²⁺-C₂O₄²⁻ system has been studied systematically. K₂Sn(C₂O₄)₂·H₂O was successfully synthesized by the hydrothermal reaction method. Regrettably, however, although K₂Sn(C₂O₄)₂·H₂O consists of Sn²⁺-polyhedra

and C₂O₄²⁻ groups, it features a 0D anionic structure. We noticed that F⁻ ions are also widely considered to be excellent chemical scissors. When the F⁻ ions are introduced into the cation-centered polyhedra(M-polyhedra) of oxygenates, the other oxygen ligands are squeezed and moved toward the equator, which not only decrease the symmetry of the polyhedra, but also facilitate the extension of the polyhedra by sharing oxygen atoms. The C-F bond, which is generally shorter than the M-O bond, could cut the connecting bridge of chain to chain. As a result, F⁻ was considered for introduction into the Sn²⁺-C₂O₄²⁻ system, and K₂Sn₂(C₂O₄)₂F₂·H₂O featuring a unique 1D anionic structure was successfully synthesized by the solution evaporation method. Fascinatingly, as the crystal structure transforms from 0D to 1D, the birefringence increases dramatically from 0.103@546 nm in K₂Sn(C₂O₄)₂·H₂O to 0.301@546 nm as expected.

Experimental section

Synthesis of K₂Sn(C₂O₄)₂·H₂O and K₂Sn₂(C₂O₄)₂F₂·H₂O

Reaction reagents: SnO (AR, 99%), K₂C₂O₄·H₂O (AR, 99.8%), SnF₂ (AR, 99%), and HF (AR, ≥40.0%). All materials were used as received and without further operation. There are some important things to follow when using HF: pay attention to ventilation, do a good job of safety protection, wear rubber acid-alkali resistant clothing and gloves, wash your hands thoroughly after use, and keep the place clean.

The compound K₂Sn(C₂O₄)₂·H₂O was synthesized by the hydrothermal reaction method. SnO (0.135 g) and K₂C₂O₄·H₂O (0.737 g) were added into H₂O (3 mL) and HF (0.1 mL). After 20 minutes of stirring, the mixture was sealed into an autoclave with a 23 mL Teflon liner and heated at 100 °C for 5 days, and then slowly cooled down to room temperature at 6 °C h⁻¹. In order to obtain a pure compound, the reaction mixture has to be rinsed with ethanol, and dried in air.

The compound K₂Sn₂(C₂O₄)₂F₂·H₂O was gained by the solution evaporation method. A mixture of SnF₂ (0.317 g) and K₂C₂O₄·H₂O (0.252 g) with a molar ratio of 2 : 3 was dissolved in H₂O (5 mL), and the solution was reddish brown after stirring for 20 minutes. Then the solution was transferred into a refrigerator at 4 °C. After 5 days, the reaction product was washed with ethanol and dried in air. Finally, block-like crystals were obtained.

Single crystal structure determination

By using a Rigaku XtaLAB Synergy R diffractometer with graphite monochromatic Mo-Kα radiation, the single crystal data of K₂Sn(C₂O₄)₂·H₂O and K₂Sn₂(C₂O₄)₂F₂·H₂O can be obtained at 150(2) K. The structures of the two compounds were refined with SHELXL-2014.⁴² We used the program PLATON⁴³ to inspect the structure, and no higher symmetries could be found. The related crystal data and structure refinement of the two compounds are listed in Tables S1–S5.†

Powder X-ray Diffraction

A SmartLab powder X-ray diffractometer with Cu-K α radiation was used to gather the powder X-ray diffraction patterns for K₂Sn(C₂O₄)₂·H₂O, and K₂Sn₂(C₂O₄)₂F₂·H₂O at room temperature. The decay test conditions are as follows: the 2 θ angular range starts from 5° and stops at 70°, the scan step width is 0.02°, and the fixed time is 0.2 s. The test results show that the experimental pattern is consistent with the calculated pattern (Fig. S1†).

Thermal analysis

Thermogravimetric analysis of the two compounds was performed using NETZSCH STA-449C with a constant flow of N₂ gas and the test temperature was from room temperature to 800 °C, with a heating rate of 10 °C per min (Fig. S2†).

Infrared spectroscopy

The data of infrared (IR) spectroscopy for K₂Sn(C₂O₄)₂·H₂O and K₂Sn₂(C₂O₄)₂F₂·H₂O were recorded with a Fourier transform infrared (FTIR) spectrometer with the model number Vertex 70. The range of measurement is 4000–400 cm⁻¹. The proportion of the sample and dried KBr is about 1:100 (Fig. S4†).

UV-Vis diffuse reflectance spectroscopy

A Shimadzu UV-2600 spectrophotometer was used to record the data of UV-vis diffuse reflectance spectroscopy for the two compounds with the wavelength range of 200–800 nm at room temperature (Fig. S5†).

Birefringence measurements

Birefringence tests of K₂Sn(C₂O₄)₂·H₂O and K₂Sn₂(C₂O₄)₂F₂·H₂O were conducted on a ZEISS Axio Scope A5 polarizing microscope with a Berek compensator. The formula used to calculate the birefringence is listed as follows:

$$\Delta R = \Delta n \times d. \quad (1)$$

ΔR indicates the optical path difference, Δn refers to the birefringence, and d is the thickness of the crystal. The results of the tests are shown in Fig. S6.†

Theoretical calculations

The data of the theoretical calculations for both the compounds were calculated using a Cambridge Serial Total Energy Package (CASTEP)⁴⁴ program, which is based on density functional theory (DFT).⁴⁵ In this way, we could calculate the band structure, density of states, optical properties and so on. The Perdew–Burke–Ernzerhof (PBE)⁴⁶ functional with Generalized Gradient Approximation (GGA) was employed for all calculations. To simplify the potential energy of all the atoms, Norm-conserving Pseudopotential (NCP)⁴⁷ was adopted. The kinetic energy cutoffs for K₂Sn(C₂O₄)₂·H₂O and K₂Sn₂(C₂O₄)₂F₂·H₂O were 750 eV, and the k -points in the first Brillouin zone were 4 × 4 × 2 (K₂Sn(C₂O₄)₂·H₂O) and 2 × 3 × 2 (K₂Sn₂(C₂O₄)₂F₂·H₂O). The valences of all atoms are listed

below: H 1s¹, C 2s²2p², O 2s²2p⁴, F 2s²2p⁵, K 3s²3p⁶4s¹, Sn 4d¹⁰5s²5p².

Results and discussion

Crystal structures

The two centrosymmetric Sn²⁺-based oxalates K₂Sn(C₂O₄)₂·H₂O and K₂Sn₂(C₂O₄)₂F₂·H₂O crystallize in the triclinic space group $P\bar{1}$ (No. 2) and $P2_1/c$ (No. 14), respectively, and the crystal structure of K₂Sn(C₂O₄)₂·H₂O⁴⁸ was previously reported. Their basic functional anionic groups are planar π -conjugated [C₂O₄]²⁻ with rational bond lengths (C–O: 1.228–1.286 Å and C–C: 1.550–1.558 Å) and bond angles (O–C–O: 123.7–126.7°, O–C–C: 115.4–120.3°), which are interconnected with the cationic building modules Sn²⁺-based polyhedra and K⁺ cations to assemble crystal frameworks respectively (Fig. 1). It is interesting that the diverse coordination environments and spatial arrangements in these building blocks lead to the unique crystal structures of these two compounds.

K₂Sn(C₂O₄)₂·H₂O contains one independent Sn atom, two K atoms, four C atoms, and nine O atoms in a unit cell. The Sn atom is four coordinated with four O atoms to form a SnO₄ seesaw polyhedron with Sn–O bond distances of 2.148–2.375 Å (Fig. 1a). Each SnO₄ seesaw polyhedron is linked to two nearly perpendicular [C₂O₄]²⁻ planar groups by sharing four O atoms to form a 0D [Sn(C₂O₄)₂]²⁻ anionic structure (Fig. 1b). In addition, K⁺ cations with charge compensation and H₂O molecules are distributed in the voids of these [Sn(C₂O₄)₂]²⁻ clusters (Fig. 1c).

For the compound K₂Sn₂(C₂O₄)₂F₂·H₂O, the two independent Sn1 and Sn2 atoms are all connected with four O atoms and one F atom in a SnO₄F tetragonal pyramid with the bond length of Sn–O of 2.281–2.729 Å and that of Sn–F of 2.020–2.045 Å, respectively (Fig. 1d). The [C₂O₄]²⁻ planar groups act as bridges to connect [Sn(1)O₄F]⁷⁻ and [Sn(2)O₄F]⁷⁻ in opposite directions by sharing O atoms, constructing a 1D [Sn₂(C₂O₄)₂F₂] _{∞} ²⁻ anionic structure, and these chains are parallel to each other. The K atoms and H₂O molecules are arranged between the chains, with the K atoms playing a major role in charge-balancing (Fig. 1e and f).

Thermal analysis

The results of thermogravimetric analysis of the two title compounds are shown in Fig. S2.† The decomposition temperatures of K₂Sn(C₂O₄)₂·H₂O and K₂Sn₂(C₂O₄)₂F₂·H₂O are 40 °C and 42 °C, and the corresponding total weight loss rates are about 40% and 27%, respectively. The final decomposition products of these two compounds were tested by X-ray powder diffraction, demonstrating that the main products of the two compounds are SnO₂ and K₂SnO₃ in K₂Sn(C₂O₄)₂·H₂O and SnO₂ in K₂Sn₂(C₂O₄)₂F₂·H₂O, respectively (Fig. S3†).

Infrared spectroscopy

As shown in Fig. S4,† the IR spectra of K₂Sn(C₂O₄)₂·H₂O and K₂Sn₂(C₂O₄)₂F₂·H₂O were recorded from 4000 to 400 cm⁻¹. The

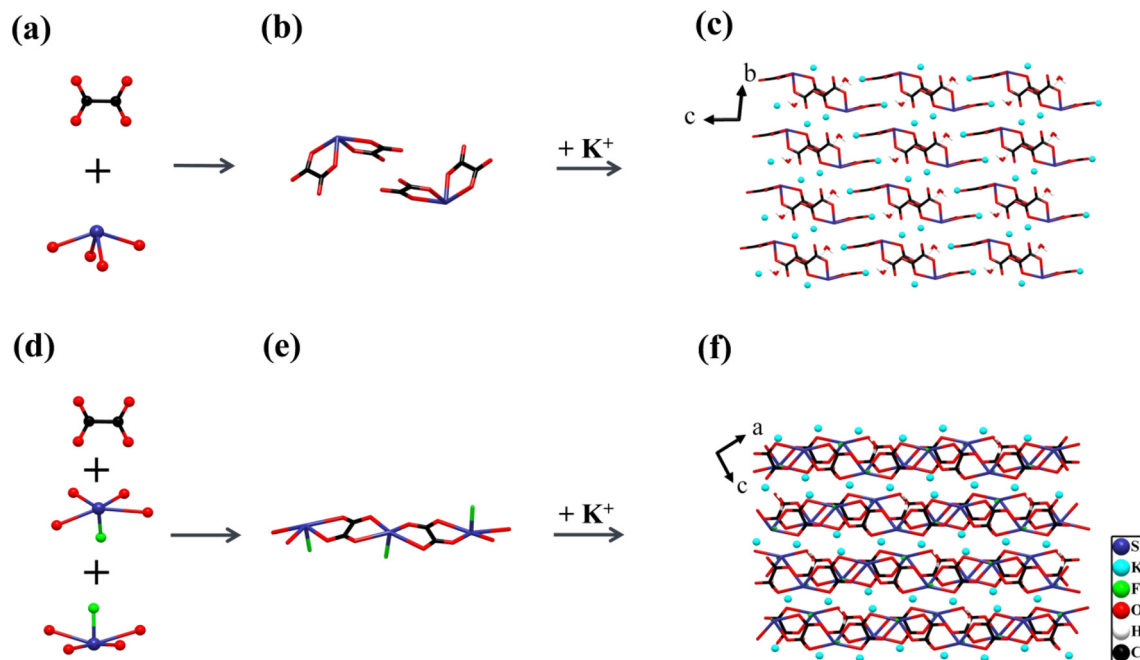


Fig. 1 (a and d) The coordination modes of Sn^{2+} and planar $[\text{C}_2\text{O}_4]^{2-}$ groups; (b and e) the different connection modes between Sn^{2+} -polyhedra and $[\text{C}_2\text{O}_4]^{2-}$ groups; (c and f) the structure of $\text{K}_2\text{Sn}(\text{C}_2\text{O}_4)_2\cdot\text{H}_2\text{O}$ and $\text{K}_2\text{Sn}_2(\text{C}_2\text{O}_4)_2\text{F}_2\cdot\text{H}_2\text{O}$ along the a -axis and b -axis, respectively.

peaks from 3416 cm^{-1} to 3709 cm^{-1} are the stretching vibrations of H_2O . The peaks at 1637 cm^{-1} and 1642 cm^{-1} are identified as the stretching vibrations of $\text{C}=\text{O}$ bonds. The bands at 1485 cm^{-1} , 1421 cm^{-1} , 1273 cm^{-1} , and 1047 cm^{-1} can be ascribed to $\text{C}-\text{O}$ stretching vibrations. The peaks at about 887 cm^{-1} , 783 cm^{-1} and 786 cm^{-1} are considered to be the stretching vibrations of $\text{C}-\text{C}$ and bending vibrations of $\text{O}-\text{C}=\text{O}$ bonds. The characteristic absorption bands at around 493 cm^{-1} and 487 cm^{-1} belong to the vibrations of $\text{Sn}-\text{F}$ bonds for $\text{K}_2\text{Sn}_2(\text{C}_2\text{O}_4)_2\text{F}_2\cdot\text{H}_2\text{O}$. All of the vibrations are in agreement with previously reported spectra in the literature.^{18,41,49–51}

UV-Vis diffuse reflectance spectroscopy

The UV-vis diffuse reflectance spectra of $\text{K}_2\text{Sn}(\text{C}_2\text{O}_4)_2\cdot\text{H}_2\text{O}$ and $\text{K}_2\text{Sn}_2(\text{C}_2\text{O}_4)_2\text{F}_2\cdot\text{H}_2\text{O}$ are shown in Fig. S5.† It reveals that the band gaps of $\text{K}_2\text{Sn}(\text{C}_2\text{O}_4)_2\cdot\text{H}_2\text{O}$ and $\text{K}_2\text{Sn}_2(\text{C}_2\text{O}_4)_2\text{F}_2\cdot\text{H}_2\text{O}$ are 3.74 eV and 3.21 eV, and the corresponding UV absorption cutoff edges are 286 nm and 310 nm, respectively, illustrating that the two compounds can be used in the ultraviolet region.

Birefringence measurements

A ZEISS Axio A5 polarizing microscope was used to measure the birefringence of $\text{K}_2\text{Sn}(\text{C}_2\text{O}_4)_2\cdot\text{H}_2\text{O}$ and $\text{K}_2\text{Sn}_2(\text{C}_2\text{O}_4)_2\text{F}_2\cdot\text{H}_2\text{O}$ at 546 nm. The retardation and thickness of these two are 762 nm, 1803 nm and $7.433\text{ }\mu\text{m}$, $5.993\text{ }\mu\text{m}$, respectively. After substituting these values into eqn (1), the birefringence values of $\text{K}_2\text{Sn}(\text{C}_2\text{O}_4)_2\cdot\text{H}_2\text{O}$ and $\text{K}_2\text{Sn}_2(\text{C}_2\text{O}_4)_2\text{F}_2\cdot\text{H}_2\text{O}$ were obtained as 0.103 and 0.301 at 546 nm, respectively (Fig. 2a and b). In addition, the refractive indices of the compounds are calculated and presented in Fig. 2c and d. The results show that

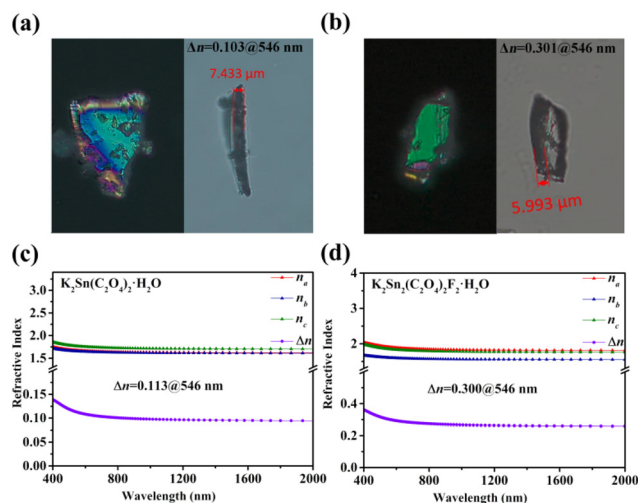


Fig. 2 (a and b) Experimental birefringence at 546 nm; (c and d) calculated refractive index for $\text{K}_2\text{Sn}(\text{C}_2\text{O}_4)_2\cdot\text{H}_2\text{O}$ and $\text{K}_2\text{Sn}_2(\text{C}_2\text{O}_4)_2\text{F}_2\cdot\text{H}_2\text{O}$.

$\text{K}_2\text{Sn}(\text{C}_2\text{O}_4)_2\cdot\text{H}_2\text{O}$ is positive biaxial crystals ($n_z - n_y > n_y - n_x$) and $\text{K}_2\text{Sn}_2(\text{C}_2\text{O}_4)_2\text{F}_2\cdot\text{H}_2\text{O}$ is negative biaxial crystals ($n_z - n_y < n_y - n_x$). The calculated birefringence of these compounds is 0.113 and 0.300 at 546 nm, respectively, which closely match the experimental values. It is obvious that $\text{K}_2\text{Sn}_2(\text{C}_2\text{O}_4)_2\text{F}_2\cdot\text{H}_2\text{O}$ has a significantly enhanced birefringence compared to $\text{K}_2\text{Sn}(\text{C}_2\text{O}_4)_2\cdot\text{H}_2\text{O}$, which surpasses that of traditional birefringent crystals such as LiNbO_3 ($0.074@546\text{ nm}$),⁵² MgF_2 ($0.012@532\text{ nm}$),⁶ $\alpha\text{-BBO}$ ($0.122@546\text{ nm}$),⁵ CaCO_3 ($0.172@532\text{ nm}$),⁸ YVO_4 ($0.204@532\text{ nm}$),⁷ and TiO_2

(0.256@546 nm),⁵³ and some reported oxalate crystals, *e.g.*, (CN₄H₇)SbC₂O₄F₂(H₂O)_{0.5} (0.126@546 nm),⁵⁴ K₂Sb₂C₂O₄F₅ (0.170@546 nm),³³ Rb₂C₂O₄ (0.201@1064 nm),⁵⁵ and (NH₄)₂SbC₂O₄Cl₃ (0.270@546 nm).⁵⁶ Besides, the title compounds are preferred in terms of stable physicochemical properties, suggesting that Sn²⁺-oxalates can be used as potential birefringent materials.

Molecular engineering regulates birefringence

As described above, these two compounds employ the same birefringence-active FMs, *i.e.*, π -conjugated [C₂O₄]²⁻ planar groups and Sn²⁺ cations with SCALP, but their birefringence changes tremendously, which may indicate that the spatial arrangement of the FMs has a significant effect on the birefringence. By comparing the structural features of the two compounds, the only difference lies in the construction of the FMs, namely a 0D [Sn(C₂O₄)₂]²⁻ anionic structure in K₂Sn(C₂O₄)₂·H₂O and a 1D [Sn₂(C₂O₄)₂F₂]_∞²⁻ anionic structure in K₂Sn₂(C₂O₄)₂F₂·H₂O. Then, the spatial arrangement characteristics of these two are analyzed in detail. The lone pair electrons of the Sn²⁺ cation act as chemical scissors to shear the tendency to connect to its ipsilateral side, so that all O ligands of the Sn are evenly distributed on the other side of the lone pair electrons in K₂Sn(C₂O₄)₂·H₂O. As a result, the [C₂O₄]²⁻ groups connected to the SnO₄ seesaw polyhedron by shared O atoms are arranged non-coplanar, and inconsistent orientations between [C₂O₄]²⁻ groups and lone pair electrons lead to a moderate birefringence of 0.103@546 nm (Fig. 3a and b). K₂Sn₂(C₂O₄)₂F₂·H₂O has not only the chemical scissors of the lone pair electrons, but also other chemical scissors of the fluorine atoms. The shorter Sn–F bonds keep the chain from being linked to another chain by sharing F atoms in one direction, successfully forming the [Sn₂(C₂O₄)₂F₂]_∞²⁻ chains in K₂Sn₂(C₂O₄)₂F₂·H₂O. The 1D anionic structure is widely recognized as a structural mode with great potential to produce large birefringence, such as Na₂Sb₂(C₂O₄)F₆ and Cs₂Sb₂(C₂O₄)₂F₄·H₂O. In addition, the introduced F ligand occupies the space around Sn²⁺, forcing the four O ligands to

shift toward the equatorial position of the Sn atom. Naturally, the [C₂O₄]²⁻ groups attached to the Sn²⁺-polyhedra also tend to be arranged in parallel, further enabling effective superposition of π -conjugated orbitals. In K₂Sn₂(C₂O₄)₂F₂·H₂O, there is only one wave-like [Sn₂(C₂O₄)₂F₂]_∞²⁻ chain consisting of alternating linkages of a SnO₄F tetragonal pyramid and [C₂O₄]²⁻ groups named chain A. As expected, all the [C₂O₄]²⁻ groups in one chain are arranged with near coplanarity, and all of the SnO₄F tetragonal pyramids stand neatly. Subsequently, all chains A are arranged strictly parallel in the *ac* plane (Fig. 3c and d), with the lone pair electrons of Sn²⁺ and the π -conjugated electrons of the [C₂O₄]²⁻ group lying in the same plane. Such a regular planar arrangement and uniform orientation result in K₂Sn₂(C₂O₄)₂F₂·H₂O exhibiting a large birefringence of 0.301@546 nm, which is approximately 2.9 times larger than that of K₂Sn(C₂O₄)₂·H₂O. Thus, achieving a parallel and consistent alignment of birefringence-active FMs may be an effective approach to obtain significantly enhanced birefringence.

In this work, synergistic interactions of Sn²⁺ cations with SCALP and π -conjugated [C₂O₄]²⁻ anion groups makes the birefringence vary dramatically from 0.103@546 nm of K₂Sn(C₂O₄)₂·H₂O to 0.301@546 nm of K₂Sn₂(C₂O₄)₂F₂·H₂O based on the structure–property relationship. To investigate in depth the contribution of birefringence-active FMs to the birefringence of the compounds, a detailed analysis of the microscopic mechanism is further conducted. First, the optical properties of all FMs were calculated using the Gaussian 09 package. As shown in Fig. 4a, the results indicate that the polarization anisotropy of the SnO₄F tetragonal pyramid is significantly greater than that of the SnO₄ seesaw polyhedron as expected. For [C₂O₄]²⁻ groups with slight flexibility, the dihedral angles between the two [CO₂] in one [C₂O₄]²⁻ group range from 1.512° to 6.736° in the title compounds. Therefore, the small degree of distortion of [C₂O₄]²⁻ groups has a negligible effect on their optical anisotropy (Table S6†). Obviously, the individual birefringence-active FM with superior polarization anisotropy is not the only essential factor to obtain a large birefringence, since birefringence originates from the effective superposition of microscopic polarization anisotropies of all birefringence-active FMs, which is reflected in their spatial orientation and density. In this work, the calculated refractive index shows that the two compounds are biaxial crystals, and the birefringence can be obtained by $\Delta n = n_z - n_x$. It can be speculated that the larger the birefringence-active FMs acting on the optical principal axis Z or the smaller on the X-axis, the more favorable it is to obtain a large birefringence. Therefore, the relationship between the YZ plane (*ac* plane for K₂Sn(C₂O₄)₂·H₂O, *ac* plane for K₂Sn₂(C₂O₄)₂F₂·H₂O) and the orientation of the lone pair electrons in the Sn²⁺ cations and the C₂O₄²⁻ planes, respectively, is essential for exploring their contribution to birefringence. In Sn²⁺ cations with a SCALP, the lone pair electron is located on the opposite sides of the vector sum of the all Sn–O and/or Sn–F bonds of Sn²⁺-based polyhedra, and the angle it forms with the YZ plane is defined as α . Ideally, the lone pair electron would make the largest con-

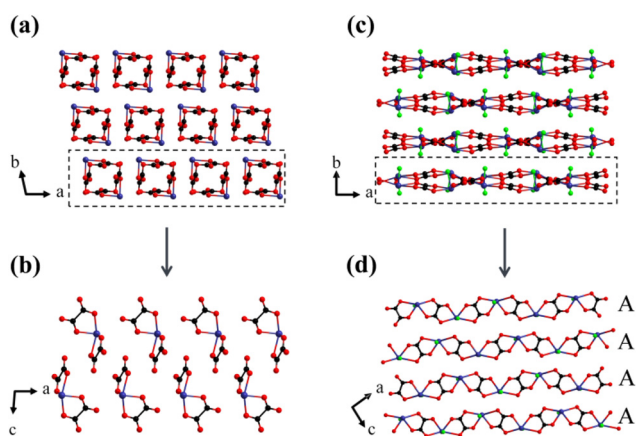


Fig. 3 The different arrangements of Sn²⁺-[C₂O₄]²⁻ groups in K₂Sn(C₂O₄)₂·H₂O (a and b) and K₂Sn₂(C₂O₄)₂F₂·H₂O (c and d).

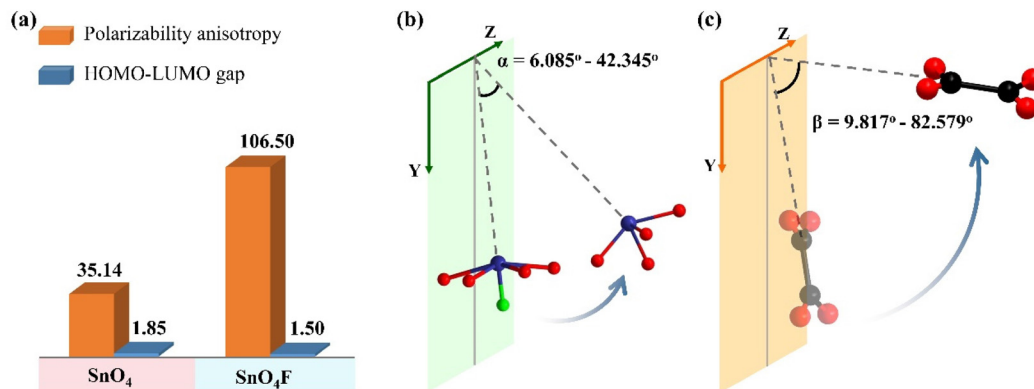


Fig. 4 (a) The polarizability anisotropy and HOMO–LUMO gap of Sn²⁺-polyhedra (SnO₄ for K₂Sn(C₂O₄)₂·H₂O and SnO₄F for K₂Sn₂(C₂O₄)₂F₂·H₂O); (b) the angles between the lone pair electron of Sn²⁺ and the YZ plane; and (c) the dihedral angles between the [C₂O₄]²⁻ plane and YZ plane in K₂Sn(C₂O₄)₂·H₂O and K₂Sn₂(C₂O₄)₂F₂·H₂O.

tribution to the birefringence when α is equal to 0°, *i.e.*, the lone pair electron is completely parallel to the YZ plane. Here, the $\cos \alpha$ values reveal that the contribution of the SnO₄ seesaw polyhedron in K₂Sn(C₂O₄)₂·H₂O to birefringence is significantly smaller than that of the SnO₄F tetragonal pyramid in K₂Sn₂(C₂O₄)₂F₂·H₂O (Fig. 4b) (Table S7[†]). In C₂O₄²⁻ groups, the π -conjugated electrons that delocalized over the group plane are substantially responsible for the optical properties, so the anisotropic polarizability is very weak in the out-of-plane direction, especially perpendicular to the C₂O₄²⁻ plane, and strong in the plane direction. Subsequently, the β is adopted to describe the dihedral angle between the C₂O₄²⁻ plane and the YZ plane, which varies abundantly in the two compounds. According to the $\cos \beta$ values of the two compounds in Fig. 4c, Table S7[†], the order of contribution of C₂O₄²⁻ groups to birefringence is completely the same as that of Sn²⁺-polyhedra. Further considering the density of birefringence-active FMs in a unit cell, the contributions of π -conjugated C₂O₄²⁻ anion groups and Sn²⁺-based polyhedra with SCALP to birefringence exhibit corresponding increasing trends of $0.0047 < 0.0066$ and $0.0030 < 0.0067$ in K₂Sn(C₂O₄)₂·H₂O and K₂Sn₂(C₂O₄)₂F₂·H₂O, respectively. Unsurprisingly, the result confirms the previous conclusion that the contribution from the C₂O₄²⁻ anion groups and Sn²⁺-polyhedra is almost equally responsible for the birefringence of the compounds. Furthermore, the result is consistent with K₂Sn₂(C₂O₄)₂F₂·H₂O having a large birefringence, followed by K₂Sn(C₂O₄)₂·H₂O. Thus, the relationship between birefringence and the spatial arrangement of FMs in this work provides an idea to predict the birefringence of compounds containing lone pair electrons and/or π -conjugated planar groups.

Theoretical calculations

In order to further understand the structure–property relationship of K₂Sn(C₂O₄)₂·H₂O and K₂Sn₂(C₂O₄)₂F₂·H₂O, the electronic band structure, total and partial density of states (DOS) and electronic density differences were calculated based on the DFT method. The calculated band gaps for K₂Sn

(C₂O₄)₂·H₂O and K₂Sn₂(C₂O₄)₂F₂·H₂O are 3.00 eV and 2.29 eV, which are 0.74 eV, and 0.92 eV smaller than the experimental results, respectively (Fig. 5a and d). The reason for the underestimation of the calculated value is usually attributed to the utilization of the DFT-GGA method.⁵⁷

The data of Total Density of States (TDOS) and Partial Density of States (PDOS) for the two title compounds in Fig. 5b and e can prove the contributions of atomic orbitals to the bands. For the valence band (VB) from –10 eV to the Fermi level, the contributions are attributed to the H-1s, C-2s, C-2p, O-2s, O-2p, K-4p, Sn-5s, and Sn-5p states in K₂Sn(C₂O₄)₂·H₂O and the H-1s, C-2s, C-2p, O-2s, O-2p, F-2p, K-4p, Sn-5s, and Sn-5p states are the main contributors in K₂Sn₂(C₂O₄)₂F₂·H₂O. For the conduction band (CB), the H-1s, C-2s, C-2p, O-2p, K-4s, K-4p, Sn-5s, and Sn-5p states are the main contributors in K₂Sn(C₂O₄)₂·H₂O and K₂Sn₂(C₂O₄)₂F₂·H₂O. In partial DOS, for K₂Sn(C₂O₄)₂·H₂O, it is clearly known that there are overlaps between C-2s, C-2p, Sn-5s, and Sn-5p states and O-2s and O-2p states, indicating the presence of C–O and Sn–O covalent bonds in this compound. For K₂Sn₂(C₂O₄)₂F₂·H₂O, the C-2s, C-2p, Sn-5s, and Sn-5p states overlap with the O-2s, O-2p, and F-2p states, illustrating the presence of C–O, Sn–O, and Sn–F covalent bonds in these compounds. For the two compounds, it is quite clear that the electron orbitals near the Fermi level are composed of C-2s, C-2p, Sn-5s, Sn-5p, O-2p (K₂Sn(C₂O₄)₂·H₂O), C-2s, C-2p, Sn-5s, Sn-5p, O-2p, and F-2p (K₂Sn₂(C₂O₄)₂F₂·H₂O), respectively. This shows that the linear optical properties of the two compounds are mainly derived from the synergy of the C₂O₄²⁻ group and Sn²⁺-based polyhedra. Furthermore, in comparison with K₂Sn(C₂O₄)₂·H₂O, the birefringence can be further enhanced due to the neat arrangement of the 1D [Sn₂(C₂O₄)₂F₂]_∞²⁻ anionic structure caused by the scissor effect of the F atom with greater electronegativity in K₂Sn₂(C₂O₄)₂F₂·H₂O. In the electron density difference maps of the two compounds (Fig. 5c and f), red electronic clouds are observed around the Sn²⁺ cations and C₂O₄²⁻ planar groups, indicating that the lone pair electrons are stereoactive in Sn²⁺-polyhedra and the strong interaction between C and O atoms

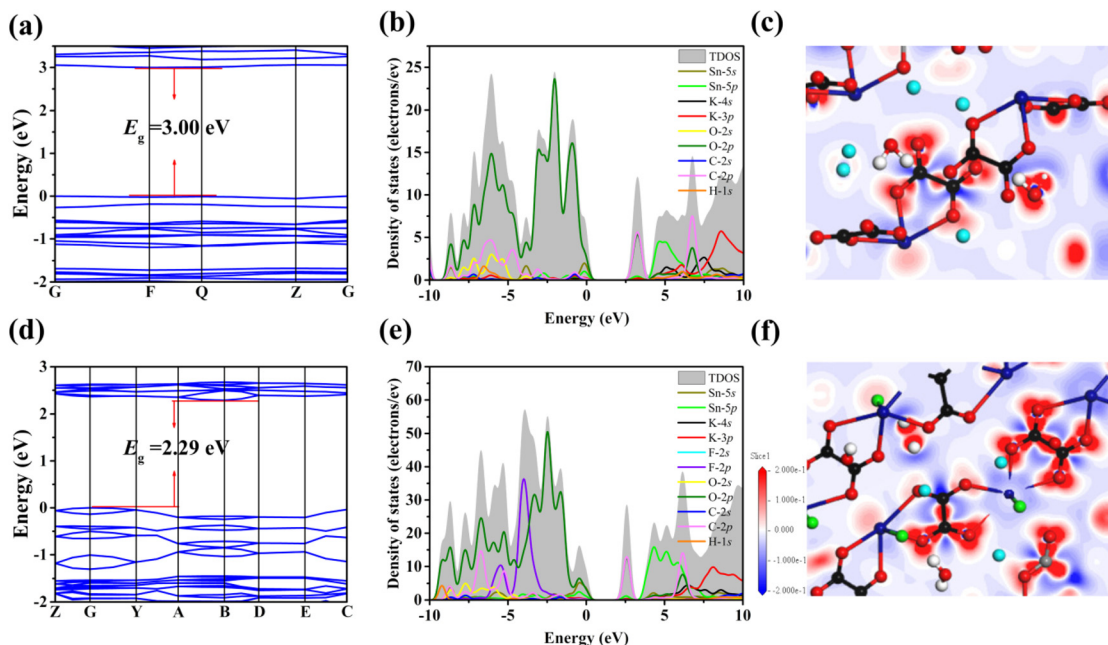


Fig. 5 (a and d) Calculated band structures; (b and e) total and partial density of states; and (c and f) electron density difference maps for $\text{K}_2\text{Sn}(\text{C}_2\text{O}_4)_2 \cdot \text{H}_2\text{O}$ and $\text{K}_2\text{Sn}_2(\text{C}_2\text{O}_4)_2\text{F}_2 \cdot \text{H}_2\text{O}$.

is charge transfer in the $\text{C}_2\text{O}_4^{2-}$ planar groups. The result further verified that the large birefringence of the two compounds originated from synergetic interactions of the $\text{C}_2\text{O}_4^{2-}$ groups and the Sn^{2+} polyhedra.

Conclusions

In brief, $\text{K}_2\text{Sn}(\text{C}_2\text{O}_4)_2 \cdot \text{H}_2\text{O}$ and $\text{K}_2\text{Sn}_2(\text{C}_2\text{O}_4)_2\text{F}_2 \cdot \text{H}_2\text{O}$ were successfully synthesized, in which Sn^{2+} cations with SCALP and π -conjugated $\text{C}_2\text{O}_4^{2-}$ anion groups were employed simultaneously to construct a 0D $[\text{Sn}(\text{C}_2\text{O}_4)_2]^{2-}$ anionic structure, and a 1D $[\text{Sn}_2(\text{C}_2\text{O}_4)_2\text{F}_2]_{\infty}^{2-}$ anionic structure, respectively. Significantly, with the increase in dimensionality, the birefringence successfully increases from 0.103@546 nm in $\text{K}_2\text{Sn}(\text{C}_2\text{O}_4)_2 \cdot \text{H}_2\text{O}$ to 0.301@546 nm in $\text{K}_2\text{Sn}_2(\text{C}_2\text{O}_4)_2\text{F}_2 \cdot \text{H}_2\text{O}$. Detailed structural and property analysis confirmed that the rational molecular engineering of the birefringence-active FMs can induce strong optical anisotropy. The significant experimental results provide the prominent UV birefringent crystals and a meaningful strategy to design novel functional materials with large birefringence.

Author contributions

L. Y. Ren: conceptualization, methodology, investigation, writing – original draft, and writing – review & editing. Y. Q. Zhou and D. J. Gao: data curation. L. L. Cao: formal analysis, project administration, resources, and writing – review & editing. L. H. Cheng: characterization analysis. X. Y. Zhou: investigation. J. X. Ren: theoretical calculation. G. H. Zou and

L. Huang: resources and supervision. X. H. Dong: conceptualization and investigation.

Conflicts of interest

There are no conflicts to declare.

Acknowledgements

The authors thank Dr Daichuan Ma at Analytical and Testing Center, Sichuan University for technical help in the Material Studio calculations. This work was supported by the National Natural Science Foundation of China (Grant No. 22201195, 22122106, 22071158, and 21971171), Natural Science Foundation of Sichuan Province (2023NSFSC1066) and the Fundamental Research Funds from Sichuan University (2021SCUNL101).

References

- X. L. Chen, B. B. Zhang, F. F. Zhang, Y. Wang, M. Zhang, Z. H. Yang, K. R. Poeppelmeier and S. L. Pan, Designing an excellent deep-ultraviolet birefringent material for light polarization, *J. Am. Chem. Soc.*, 2018, **140**, 16311–16319.
- Z. Y. Xie, L. G. Sun, G. Z. Han and Z. Z. Gu, Optical switching of a birefringent photonic crystal, *Adv. Mater.*, 2008, **20**, 3601–3604.
- S. J. Han, C. M. Huang, A. Tudi, S. S. Hu, Z. H. Yang and S. L. Pan, β - $\text{CsB}_9\text{O}_{14}$: a triple-layered borate with edge-

- sharing BO_4 tetrahedra exhibiting a short cutoff edge and a large birefringence, *Chem. – Eur. J.*, 2019, **25**, 11614–11619.
- 4 Z. L. Gao, Q. Wu, X. T. Liu, Y. X. Sun and X. T. Tao, Biaxial crystal $\alpha\text{-BaTeMo}_2\text{O}_9$: theory study of large birefringence and wide-band polarized prisms design, *Opt. Express*, 2015, **23**, 3851–3860.
 - 5 G. Q. Zhou, J. Xu, X. D. Chen, H. Y. Zhong, S. T. Wang, K. Xu, P. Z. Deng and F. X. Gan, Growth and spectrum of a novel birefringent $\alpha\text{-BaB}_2\text{O}_4$ crystal, *J. Cryst. Growth*, 1998, **191**, 517–519.
 - 6 F. Sedlmeir, R. Zeltner, G. Leuchs and H. G. L. Schwefel, High-Q MgF_2 whispering gallery mode resonators for refractometric sensing in aqueous environment, *Opt. Express*, 2014, **22**, 30934–30942.
 - 7 H. T. Luo, T. Tkaczyk, E. L. Dereniak, K. Oka and R. Sampson, High birefringence of the yttrium vanadate crystal in the middle wavelength infrared, *Opt. Lett.*, 2006, **31**, 616–618.
 - 8 G. Ghosh, Dispersion-equation coefficients for the refractive index and birefringence of calcite and quartz crystals, *Opt. Commun.*, 1999, **163**, 95–102.
 - 9 G. Peng, C. S. Lin, H. X. Fan, K. C. Chen, B. X. Li, G. Zhang and N. Ye, $\text{Be}_2(\text{BO}_3)(\text{IO}_3)$: the first anion-mixed van der Waals member in the $\text{KBe}_2\text{BO}_3\text{F}_2$ family with a very strong second harmonic generation response, *Angew. Chem., Int. Ed.*, 2021, **60**, 17415–17418.
 - 10 G. H. Zou, Z. E. Lin, H. M. Zeng, H. Jo, S. J. Lim, T. S. You and K. M. Ok, $\text{Cs}_3\text{VO}(\text{O}_2)_2\text{CO}_3$: an exceptionally thermostable carbonatoperoxovanadate with an extremely large second-harmonic generation response, *Chem. Sci.*, 2018, **9**, 8957.
 - 11 G. H. Zou, H. Jo, S. J. Lim, T. S. You and K. M. Ok, $\text{Rb}_3\text{VO}(\text{O}_2)_2\text{CO}_3$: a four-in-one carbonatoperoxovanadate exhibiting an extremely strong second-harmonic generation response, *Angew. Chem., Int. Ed.*, 2018, **57**, 8619–8622.
 - 12 R. K. Li and Y. Y. Ma, Chemical engineering of a birefringent crystal transparent in the deep UV range, *CrystEngComm*, 2012, **14**, 5421–5424.
 - 13 W. J. Xie, Z. Fang and J. G. Mao, $\text{Ba}_6\text{Zn}_6(\text{B}_3\text{O}_6)_6(\text{B}_6\text{O}_{12})$: barium zinc borate contains π -conjugated $[\text{B}_3\text{O}_6]^{3-}$ anions and $[\text{B}_6\text{O}_{12}]^{6-}$ anion with edge-sharing BO_4 tetrahedra, *Inorg. Chem.*, 2022, **61**, 18260–18266.
 - 14 Z. Li, F. Liang, Y. W. Guo, Z. S. Lin, J. Y. Yao, G. C. Zhang, W. L. Yin, Y. C. Wu and C. T. Chen, $\text{Ba}_2\text{M}(\text{C}_3\text{N}_3\text{O}_3)_2$ ($\text{M}=\text{Mg}$, Ca): potential UV birefringent materials with strengthened optical anisotropy originating from the $(\text{C}_3\text{N}_3\text{O}_3)^{3-}$ group, *J. Mater. Chem. C*, 2018, **6**, 12879.
 - 15 L. L. Cao, H. T. Tian, D. H. Lin, C. S. Lin, F. Xu, Y. L. Han, T. Yan, J. D. Chen, B. X. Li, N. Ye and M. Luo, A flexible functional module to regulate ultraviolet optical nonlinearity for achieving a balance between a second-harmonic generation response and birefringence, *Chem. Sci.*, 2022, **13**, 6990.
 - 16 X. P. Shi, W. B. Zhang, W. B. Cai, S. J. Han, Z. H. Yang and S. Pan, $\text{Li}_3\text{La}_2(\text{BO}_3)_3$ and $\text{Li}_{1.75}\text{Na}_{1.25}\text{La}_2(\text{BO}_3)_3$: a great enhancement in birefringence induced by optimal arrangement of π -Conjugated $[\text{BO}_3]$ Units, *Inorg. Chem.*, 2021, **60**, 12565–12572.
 - 17 W. B. Cai, J. Q. Chen, S. L. Pan and Z. H. Yang, Enhancement of band gap and birefringence induced via π -conjugated chromophore with “tail effect”, *Inorg. Chem. Front.*, 2022, **9**, 1224–1232.
 - 18 M. Aibibula, L. Wang and S. Z. Huang, $\text{Rb}_3\text{Na}(\text{H}_2\text{C}_3\text{N}_3\text{O}_3)_4 \cdot 3\text{H}_2\text{O}$ with Large Birefringence, *ACS Omega*, 2019, **4**, 22197–22202.
 - 19 Z. Z. Zhang, Y. Wang, H. Li, Z. H. Yang and S. L. Pan, $\text{BaB}_8\text{O}_{12}\text{F}_2$: a promising deep-UV birefringent material, *Inorg. Chem. Front.*, 2019, **6**, 546.
 - 20 H. T. Qiu, F. M. Li, C. C. Jin, J. J. Lu, Z. H. Yang, S. L. Pan and M. Mutailipu, $(\text{N}_2\text{H}_6)[\text{HPO}_3\text{F}]_2$: maximizing the optical anisotropy of deep-ultraviolet fluorophosphates, *Chem. Commun.*, 2022, **58**, 5594.
 - 21 K. C. Chen, C. S. Lin, J. D. Chen, G. S. Yang, H. T. Tian, M. Luo, T. Yan, Z. G. Hu, J. Y. Wang, Y. C. Wu, N. Ye and G. Peng, Intense d-p hybridization in Nb_3O_{15} tripolymer induced the largest second harmonic generation response and birefringence in germanates, *Angew. Chem., Int. Ed.*, 2023, **62**, e202217039.
 - 22 J. Moon and K. M. Ok, (R)- and (S)- $[\text{C}_8\text{H}_{10}\text{NO}_3]_2[\text{NbOF}_5]$: noncentrosymmetric niobium oxyfluorides with large optical anisotropy, *Inorg. Chem. Front.*, 2022, **9**, 2498–2507.
 - 23 M. Aibibula, J. Y. Guo, J. Han, A. Tudi, Z. H. Yang and S. L. Pan, $\text{BaTi}(\text{BO}_3)_2$: an excellent birefringent material with highly coplanar isolated $[\text{BO}_3]$ groups, *New J. Chem.*, 2021, **45**, 7065.
 - 24 J. Y. Guo, A. Tudi, S. J. Han, Z. H. Yang and S. L. Pan, $\text{Sn}_2\text{PO}_4\text{I}$: an excellent birefringent material with giant optical anisotropy in non π -conjugated phosphate, *Angew. Chem., Int. Ed.*, 2021, **60**, 24901–24904.
 - 25 Y. L. Deng, L. Huang, X. H. Dong, L. Wang, K. M. Ok, H. M. Zeng, Z. E. Lin and G. H. Zou, $\text{K}_2\text{Sb}(\text{P}_2\text{O}_7)\text{F}$: cairo pentagonal layer with bifunctional genes reveal optical performance, *Angew. Chem., Int. Ed.*, 2020, **59**, 21151–21156.
 - 26 Y. C. Liu, X. M. Liu, S. Liu, Q. R. Ding, Y. Q. Li, L. N. Li, S. G. Zhao, Z. S. Lin, J. H. Luo and M. C. Hong, An unprecedented antimony(III) borate with strong linear and non-linear optical responses, *Angew. Chem., Int. Ed.*, 2020, **59**, 7793–7796.
 - 27 J. Chen, C. L. Hu and J. G. Mao, $\text{LiGaF}_2(\text{IO}_3)_2$: a mixed-metal gallium iodate-fluoride with large birefringence and wide band gap, *Sci. China Mater.*, 2021, **64**, 400–407.
 - 28 S. Y. Niu, G. Joe, H. Zhao, Y. C. Zhou, T. Orvis, H. Huyan, J. Salman, K. Mahalingam, B. Urwin, J. B. Wu, Y. Liu, T. E. Tiwald, S. B. Cronin, B. M. Howe, M. Mecklenburg, R. Haiges, D. J. Singh, H. Wang, M. A. Kats and J. Ravichandran, Giant optical anisotropy in a quasi-one dimensional crystal, *Nat. Photonics*, 2018, **12**, 392–396.
 - 29 P. F. Gong, S. Z. Zhang, G. M. Song, X. M. Liu and Z. S. Lin, An unprecedented planar π -conjugated $[\text{B}_2\text{P}_5]^{5-}$ group with ultra-large birefringence and nonlinearity: an ab initio study, *Chem. Commun.*, 2020, **56**, 643.

- 30 D. Zhang, Q. Wang, L. Y. Ren, L. L. Cao, L. Huang, D. J. Gao, J. Bi and G. H. Zou, Sharp enhancement of birefringence in antimony oxalates achieved by the cation–anion synergetic interaction strategy, *Inorg. Chem.*, 2022, **61**, 12481–12488.
- 31 G. H. Zou, C. S. Lin, H. Jo, G. Nam, T. S. You and K. M. Ok, $\text{Pb}_2\text{BO}_3\text{Cl}$: a tailor-made polar lead borate chloride with very strong second harmonic generation, *Angew. Chem., Int. Ed.*, 2016, **55**, 12078–12082.
- 32 Y. Long, X. H. Dong, H. M. Zeng, Z. E. Lin and G. H. Zou, Layered perovskite-like nitrate $\text{Cs}_2\text{Pb}(\text{NO}_3)_2\text{Br}_2$ as a multifunctional optical material, *Inorg. Chem.*, 2022, **61**, 4184–4192.
- 33 Y. X. Chen, Z. X. Chen, Y. Zhou, Y. Q. Li, Y. C. Liu, Q. R. Ding, X. Chen, S. G. Zhao and J. H. Luo, An antimony (III) fluoride oxalate with large birefringence, *Chem. – Eur. J.*, 2021, **27**, 4557–4560.
- 34 Y. W. Ge, Q. Wang, F. Yang, L. Huang, D. J. Gao, J. Bi and G. H. Zou, Tin chloride sulfates $\text{A}_3\text{Sn}_2(\text{SO}_4)_{3-x}\text{Cl}_{1+2x}$ (A=K, Rb, Cs; $x=0, 1$) as multifunctional optical materials, *Inorg. Chem.*, 2021, **60**, 8322–8330.
- 35 H. X. Qi, H. Jo, X. L. Chen, J. Hong and K. M. Ok, Second-harmonic generation and photoluminescence properties of Sn(II)- and Bi(III)-based lone pair cation-pyridine dicarboxylate coordination compounds, *Inorg. Chem.*, 2020, **59**, 11554–11561.
- 36 R. A. Li, Z. Y. Zhou, Y. K. Lian, F. Jia, X. X. Jiang, M. C. Tang, L. M. Wu, J. L. Sun and L. Chen, A_2SnS_5 : a structural incommensurate modulation exhibiting strong second-harmonic generation and a high laser-induced damage threshold (A=Ba, Sr), *Angew. Chem., Int. Ed.*, 2020, **59**, 11861–11865.
- 37 J. Y. Guo, A. Tudi, S. J. Han, Z. H. Yang and S. L. Pan, $\text{Sn}_2\text{B}_5\text{O}_9\text{Cl}$: a material with large birefringence enhancement activated prepared via alkaline-earth-metal substitution by Tin, *Angew. Chem., Int. Ed.*, 2019, **58**, 17675–17678.
- 38 J. Y. Guo, A. Tudi, S. J. Han, Z. H. Yang and S. L. Pan, $\alpha\text{-SnF}_2$: a UV birefringent material with large birefringence and easy crystal growth, *Angew. Chem., Int. Ed.*, 2021, **60**, 3540–3544.
- 39 M. J. Schäfer, S. G. Jantz, F. Pielhofer and H. A. Höpfe, The very first normal-pressure tin borate $\text{Sn}_3\text{B}_4\text{O}_9$, and the intermediate $\text{Sn}_2[\text{B}_7\text{O}_{12}]\text{F}$, *Dalton Trans.*, 2019, **48**, 10398.
- 40 T. H. Tong, W. Y. Zhang, Z. H. Yang and S. L. Pan, Series of crystals with giant optical anisotropy: a targeted strategic research, *Angew. Chem., Int. Ed.*, 2021, **60**, 1332–1338.
- 41 D. Zhang, Q. Wang, T. Zheng, L. L. Cao, K. M. Ok, D. J. Gao, J. Bi, L. Huang and G. H. Zou, Cation-anion synergetic interactions achieving tunable birefringence in quasi-one-dimensional antimony(III) fluoride oxalates, *Sci. China Mater.*, 2022, **65**, 3115–3124.
- 42 G. M. Sheldrick, A short history of SHELX, *Acta Crystallogr., Sect. A: Found. Crystallogr.*, 2008, **64**, 112–122.
- 43 A. L. Spek, Single-crystal structure validation with the program PLATON, *J. Appl. Crystallogr.*, 2003, **36**, 7–13.
- 44 S. J. Clark, M. D. Segall, C. J. Pickard, P. J. Hasnip, M. I. J. Probert, K. Refson and M. C. Payne, First principles methods using CASTEP, *Z. Kristallogr. - Cryst. Mater.*, 2005, **220**, 567–570.
- 45 M. D. Segall, P. J. D. Lindan, M. J. Probert, C. J. Pickard, P. J. Hasnip, S. J. Clark and M. C. Payne, First-principles simulation: ideas, illustrations and the CASTEP code, *J. Phys.: Condens. Matter*, 2002, **14**, 2717–2744.
- 46 D. Vanderbilt, Soft self-consistent pseudopotentials in a generalized eigenvalue formalism, *Phys. Rev. B: Condens. Matter Mater. Phys.*, 1990, **41**, 7892.
- 47 K. Kobayashi, Norm-conserving pseudopotential database (NCPS97), *Comput. Mater. Sci.*, 1999, **14**, 72–76.
- 48 A. D. Christie, R. A. Howie and W. Moser, Tin(II) oxalate structures, *Inorg. Chim. Acta*, 1979, **36**, L447–L448.
- 49 L. D. Luan, J. Li, C. Chen, Z. E. Lin and H. Huang, Solvent-free synthesis of crystalline metal phosphate oxalates with a (4,6)-connected fsh topology, *Inorg. Chem.*, 2015, **54**, 9387–9389.
- 50 Y. V. Kokunov, D. G. Detkov, Y. E. Gorbunova, M. M. Ershova, Y. N. Mikhailov and Y. A. Buslaev, Crystal structure of $(\text{NH}_4)_2\text{Sn}_2\text{F}_4(\text{NO}_3)_2$: the first example of dimeric $[\text{Sn}_2\text{F}_4\text{E}_2]$ complexes in Tin(II) fluorides, *Dokl. Chem.*, 2001, **378**, 135–138.
- 51 Y. V. Kokunov, D. G. Detkov, Y. E. Gorbunova, M. M. Ershova and Y. N. Mikhailov, Synthesis and crystal structure of calcium trifluorostannate(II), *Dokl. Chem.*, 2001, **376**, 52–54.
- 52 D. E. Zelmon, D. L. Small and D. Jundt, Infrared corrected Sellmeier coefficients for congruently grown lithium niobate and 5 mol% magnesium oxide-doped lithium niobate, *J. Opt. Soc. Am.*, 1997, **14**, 3319–3322.
- 53 J. R. Devore, Refractive indices of rutile and sphalerite, *J. Opt. Soc. Am.*, 1951, **41**, 416–419.
- 54 Y. X. Chen, T. T. Zhu, Z. Y. Xiong, Y. Zhou, Y. Q. Li, Q. R. Ding, Y. C. Liu, X. Chen, S. G. Zhao and J. H. Luo, An organic-inorganic hybrid birefringent material with diverse functional groups, *Chem. Commun.*, 2021, **57**, 6668.
- 55 R. E. Dinnebier, S. Vensky, M. Jansen and J. C. Hanson, Crystal structures and topological aspects of the high-temperature phases and decomposition products of the alkali-metal oxalates $\text{M}_2[\text{C}_2\text{O}_4]$ (M=K, Rb, Cs), *Chem. – Eur. J.*, 2005, **11**, 1119–1129.
- 56 D. Zhang, Q. Wang, H. Luo, L. L. Cao, X. H. Dong, L. Huang, D. J. Gao and G. H. Zou, Deep eutectic solvents synthesis of $\text{A}_2\text{Sb}(\text{C}_2\text{O}_4)\text{Cl}_3$ (A= NH_4 , K, Rb) with superior optical performance, *Adv. Opt. Mater.*, 2023, **11**, 2202874.
- 57 J. L. Song, C. L. Hu, X. Xu, F. Kong and J. G. Mao, A facile synthetic route to a new SHG material with two types of parallel π -conjugated planar triangular units, *Angew. Chem., Int. Ed.*, 2015, **54**, 3679–3682.